ACS OMEGA

http://pubs.acs.org/journal/acsodf

Article

Biocompatible $CuInS_2$ Nanoparticles as Potential Antimicrobial, Antioxidant, and Cytotoxic Agents

Ranjan Kr. Giri,* Sunil Chaki,* Ankurkumar J. Khimani, Yati H. Vaidya, Parth Thakor, Anjali B. Thakkar, Swati J. Pandya, and Milind P. Deshpande

Cite This: *ACS Omega* 2021, 6, 26533−26544

Read Online

ACCESS | Metrics & More | Article Recommendations

ABSTRACT: A simple hydrothermal route is employed to synthesize pure copper indium disulfide (CIS) and CIS nanoparticles (NPs) mediated by various natural plant extracts. The plant extracts used to mediate are *Azadirachta indica* (neem), *Ocimum sanctum* (basil), *Cocos nucifera* (coconut), *Aloe vera* (aloe), and *Curcuma longa* (turmeric). The tetragonal unit cell structure of as-synthesized NPs is confirmed by X-ray diffraction. The analysis by energy-dispersive X-rays shows that all the samples are near-stoichiometric. The morphologies of the NPs are confirmed by high-resolution scanning and transmission modes of electron microscopy. The thermal stability of the synthesized NPs is determined by thermogravimetric analysis. The optical energy band gap is determined from the absorption spectra using Tauc's equation. The antimicrobial activity analysis and the estimation of the minimum inhibitory concentration (MIC) value of the samples are performed for *Escherichia coli*, *Pseudomonas aeruginosa*, *Proteus vulgaris*, *Enterobacter aerogenes*, and *Staphylococcus aureus* pathogens. It shows that the aloe-mediated CIS NPs possess a broad inhibitory spectrum. The best inhibitory effect is observed against *S. aureus*, whereas the least effect was exhibited against *P. vulgaris*. The least MIC value is found for aloe-mediated CIS NPs (0.300 mg/mL) against *S. aureus*, *P. aeruginosa*, and *E. aerogenes*, along with basil-mediated NPs against *E. coli*. The antioxidant activity study showed that the IC_{50} value to inhibit the scavenging activity is maximum for the control (vitamin C) and minimum for pure CIS NPs. The in vivo cytotoxicity study using brine shrimp eggs shows that the pure CIS NPs are more lethal to brine shrimp than the natural extract-mediated CIS NPs. The in vitro cytotoxicity study using the human lung carcinoma cell line (A549) shows that the IC_{50} value of turmeric extract-mediated CIS NPs is minimum (15.62 ± 1.58 μg/mL). This observation reveals that turmeric extract-mediated CIS NPs are the most potent in terms of cytotoxicity toward the A549 cell line.

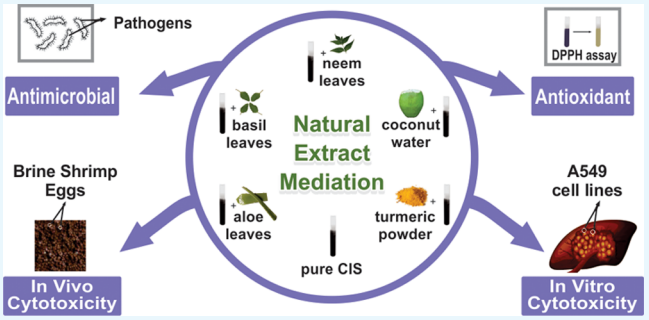

1. INTRODUCTION

Metal chalcogenide semiconductors have attracted lots of attention over the past few years due to their electrical and optical properties, which are beneficial to mankind, as an alternative to conventional semiconductors. Nanosized metal chalcogenide semiconductors show quantum confinement effects by means of shape and size control. The properties of the nanosized particles can be tuned by varying their chemical composition.[1−3] Nanostructures of various materials show excellent behavior in applications such as photodetection,[4] photocatalysis,[5] electrocatalysis,[6] energy storage anodes,[7,8] electrochemical N_2 reduction,[9] and so forth. Amid several inorganic nanoparticles (NPs), $CuInS_2$ (CIS) has received importance due to its low toxicity owing to the absence of lead and cadmium. CIS belongs to the I−III−VI_2 group having a tetragonal structure and possesses a direct band gap of ∼1.5 eV when in the bulk form.[10] The CIS NPs find applications in numerous fields including photovoltaic devices,[11,12] light-emitting diodes,[13,14] photocatalysis,[15,16] bioimaging,[17,18] and so forth. Since NPs possess a larger surface-to-volume ratio than the bulk, they efficiently interact with tissues to provide a large number of active sites, resulting in effective biological activities.[19]

Several reports are found to synthesize CIS NPs using various surfactants, capping agents, and so forth with an aim to improve efficiency. The gemini surfactant 1,10-bis(4-methyl-4-hexadecylpiperazine) controls the shape and size of the CIS microparticles/NPs to find varied applications.[20] A report states that CIS/ZnS nanocrystals passivated by cetyltrimethy-

Received: July 16, 2021
Accepted: September 16, 2021
Published: September 29, 2021

lammonium bromide enhance photostability.[21] Hybrid solar cells are fabricated using triphenyl phosphite-capped CIS conjugated with polymer 2-methoxy-5-(2′-ethyl-hexyloxy)-1,4-phenylene-vinylene in different molar ratios.[22] The CIS NPs capped with *n*-acetyl-*n*-cysteine employing a hydrothermal technique have been reported.[23] An enhanced electrical conductivity for thin films of CIS nanocrystals capped with *tert*-butylthiol has been documented.[24] The literature states that CIS NPs capped with trioctylphosphine oxide are synthesized by a hot injection method.[25] Several reports are found of biological applications due to the less toxic and ecofriendly nature of CIS NPs. Among them, chitosan-capped CIS NPs have been investigated for bioimaging applications.[26] The CIS/ZnS core−shell nanocrystals are employed as fluorescent probes for in vivo and in vitro biological imaging.[27] A study shows the good biocompatibility stability of Gd-based CIS/ZnS nanoprobes for in vitro cytotoxicity.[28] The literature states that the incorporation of plant extracts such as *Azadirachta indica* (neem),[29,30] *Ocimum sanctum* (basil),[31,32] *Cocos nucifera* (coconut),[33] *Aloe vera* (aloe),[34,35] *Curcuma longa* (turmeric),[36] and so forth during synthesis makes the NPs biocompatible. The incorporation of green extracts improves the antimicrobial, antioxidant, and cytotoxicity activities of the NPs.[37−41] Apprehending the significance of CIS NPs, the authors decided to study them for biological applications. The authors also studied the consequence of the mediation of varied natural extracts into the CIS NPs on their different properties.

The NPs' synthesis is reported by various techniques such as the sonochemical method,[42] hydrothermal method,[43] solvothermal method,[44] wet-chemical synthesis,[45] one-pot synthesis,[46] and so forth. In a previous work of the authors, it is documented that CIS NPs synthesized by the hydrothermal route are more stable than CIS NPs synthesized by the sonochemical route.[47] Therefore, the authors decided to employ a hydrothermal route for the synthesis of pure CIS and natural extract-mediated CIS NPs.

To the best of the authors' knowledge, no work has been reported on plant extract incorporation into any metal chalcogenide semiconductors. The authors synthesized pure CIS and plant extract-mediated CIS NPs using a simple hydrothermal technique. The hydrothermal synthesis mediated by plant extracts such as neem, basil, coconut, aloe, and turmeric is undertaken. The reason behind the selection of these herbal plants is the presence of nimbin, nimbidin, limonoids, and so forth[48,49] in neem leaves; linalool, 1,8-cineole, and so forth[50,51] in basil leaves; aloin, emodin, and so forth[52−54] in aloe leaves; alanine, arginine, and so forth[55,56] in coconut water, and demethoxycurcumin, 5′-methoxycurcumin, dihydrocurcumin, and so forth[57] in turmeric powder. These natural extracts amalgamate CIS NPs to show enhanced antimicrobial, antioxidant, and in vivo and in vitro cytotoxicity activities compared to that of pure CIS NPs.

2. CHARACTERIZATIONS

The unit crystal structures of the as-synthesized NPs (S1, S2, S3, S4, S5, and S6) are determined by X-ray diffraction (XRD) using a Rigaku Ultima IV powder X-ray diffractometer employing $Cu_{K\alpha}$ radiation. The stoichiometric chemical compositions of synthesized CIS NPs are determined by employing a JEOL 5610-LV for energy-dispersive X-ray analysis (EDAX). The morphology is studied by a field-emission scanning electron microscope JEOL JSM7100F. The high-resolution transmission electron microscopy (HRTEM) and selected area electron diffraction (SAED) studies are performed with a Thermo Scientific Talos F200i S/TEM instrument. The thermogravimetric (TG) analysis is accomplished using a Seiko SII-EXSTAR TG/DTA-7200 thermal analyzer. The optical properties are investigated by employing a JASCO V-730 double-beam spectrophotometer.

The XRD patterns of the synthesized CIS NPs are shown in Figure 1. The XRD is performed in the 2θ range of 10−80°.

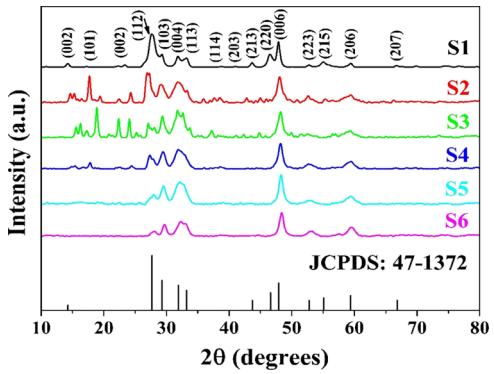

Figure 1. XRD patterns of pure CIS NPs (S1) and CIS NPs mediated by neem (S2), basil (S3), coconut (S4), aloe (S5), and turmeric (S6) extracts.

The indexing of the XRD showed the interplanar spacing and the major peak/plane matching with the standard CIS vide JCPDS Card no. 47-1372.[58] The unit cell structures determined for all the six samples are tetragonal, possessing lattice parameters $a = b = 5.51$ Å, $c = 11.32$ Å, and $\alpha = \beta = \gamma = 90°$.[59] The crystallite sizes are estimated by Scherrer's formula[60]

$$d = \frac{(0.89\lambda)}{(\beta \cos \theta)} \quad (1)$$

where λ is the wavelength of $Cu_{K\alpha}$ X-ray radiation, β is the full width at half-maximum of the peaks, and θ is the angle of diffraction. The determined average crystallite sizes of each sample are tabulated in Table 1.

Table 1. Average Crystallite Size

samples	average crystallite size (nm)
S1	21.78 ± 0.31
S2	17.21 ± 0.28
S3	18.06 ± 0.23
S4	16.27 ± 0.19
S5	16.83 ± 0.26
S6	17.59 ± 0.35

The data show that sample S1 has the largest crystallite size and the smallest size is of S4. The order of crystallinity observed from the average crystallite sizes is

S1 > S3 > S6 > S2 > S5 > S4

The observation states that the mediation of natural extracts interferes with the size of crystallites of CIS during synthesis. Thus, the incorporation of the natural extracts during hydrothermal synthesis hampers crystallization, thus decreasing the crystallite size.

https://doi.org/10.1021/acsomega.1c03795
ACS Omega 2021, 6, 26533−26544

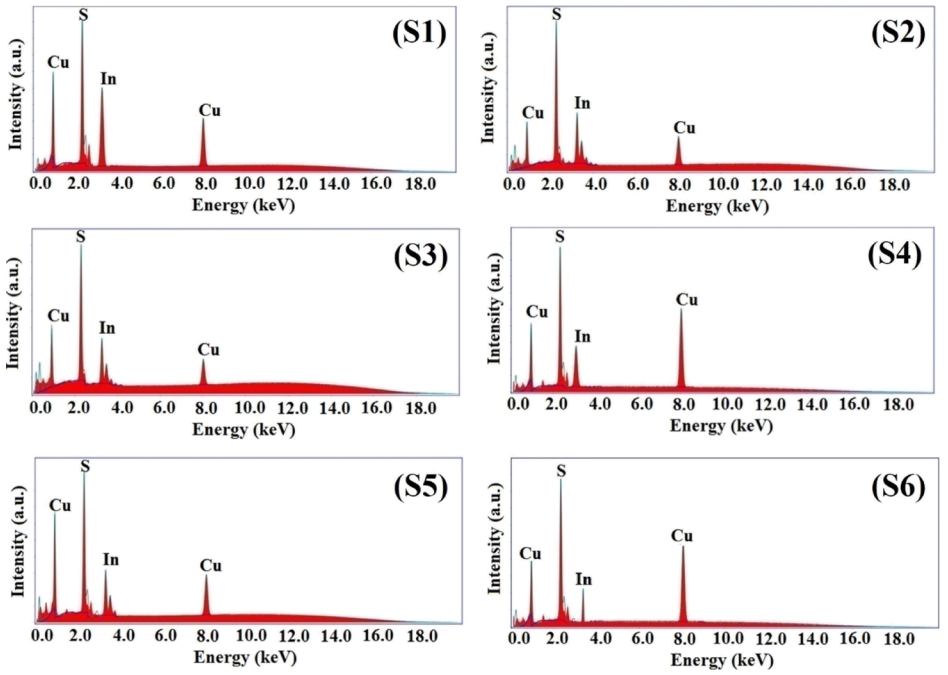

Figure 2. EDAX spectra of S1, S2, S3, S4, S5, and S6 samples.

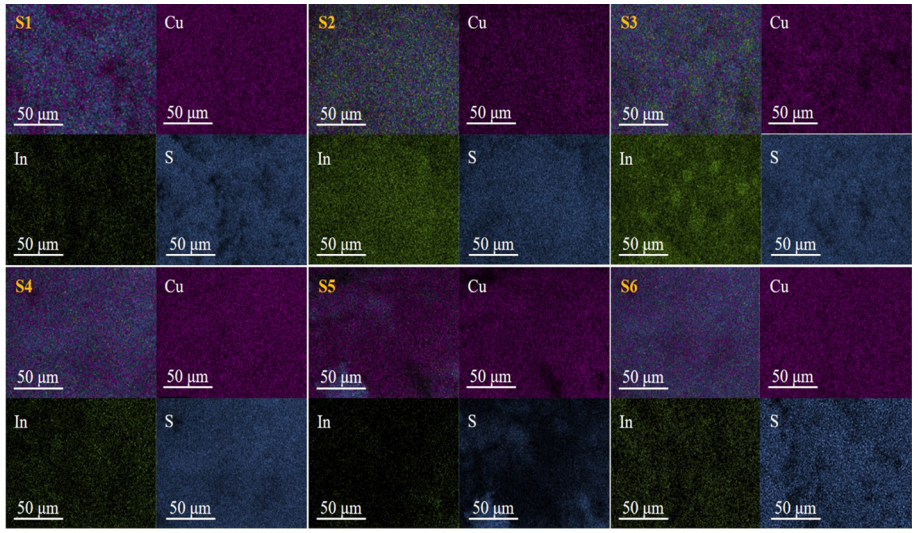

Figure 3. EDAX elemental mapping images of S1, S2, S3, S4, S5, and S6 samples.

Table 2. EDAX Data

	wt %						
elements	S1	S2	S3	S4	S5	S6	standard
Cu	25.83	25.51	25.58	25.76	25.79	25.73	26.20
In	46.67	46.19	46.16	46.28	46.23	46.09	47.35
S	27.50	28.30	28.26	27.96	27.98	28.18	26.45

The EDAX spectra and elemental mapping images of the synthesized NPs are shown in Figures 2 and 3, respectively. The obtained data along with the standard data are tabulated in Table 2.

The analysis of the data shows that all the NPs are slightly rich in S and deficient in Cu and In. In general, all the NPs are near-stoichiometric. No impurities are observed, showing the synthesized samples to be pure in composition. The EDAX observation states that the natural extract mediation does not change the composition. The basic constituent precursors decide the NP composition with a minimal role of the natural extracts.

2.3. High-Resolution Scanning Electron Microscopy. The high-resolution scanning electron microscopy (HRSEM) images of the synthesized NPs are shown in Figure 4. The observation of the images suggests that pure CIS, as shown in Figure 4a,b, has a rod-like morphology. A similar nanorod morphology is observed in the cases of neem and coconut

https://doi.org/10.1021/acsomega.1c03795
ACS Omega 2021, 6, 26533−26544

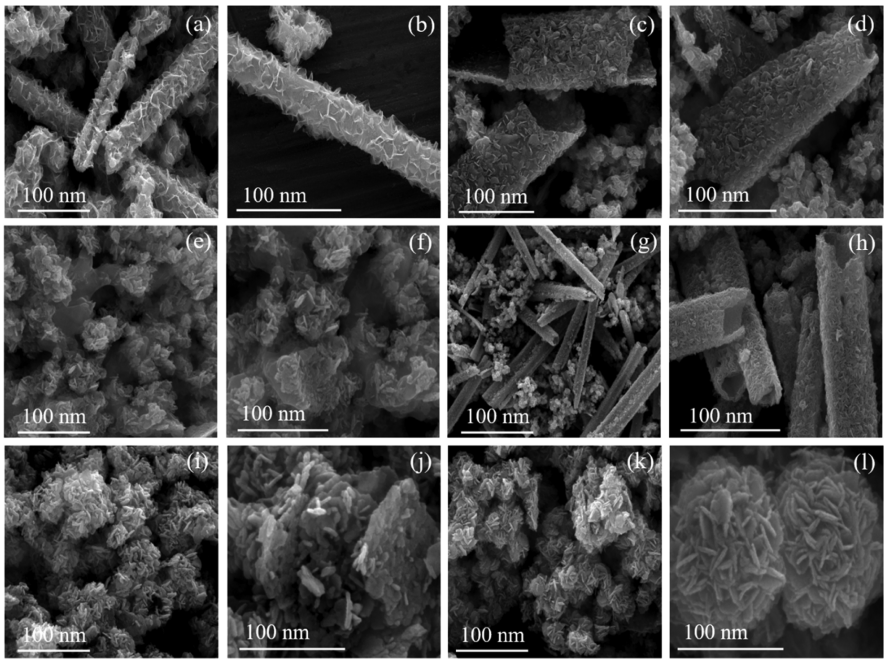

Figure 4. HRSEM images of (a,b) S1, (c,d) S2, (e,f) S3, (g,h) S4, (i,j) S5, and (k,l) S6.

extract mediation, Figure 4c,d,g,h. The incorporation of basil, aloe, and turmeric extracts changes the morphology from nanorods to sorted nanoplates, Figure 4e,f,i,j,k,l.

2.4. High-Resolution Transmission Electron Microscopy. The high-resolution transmission electron microscopy (HRTEM) images of the six synthesized NPs are shown in Figure 5a,d,g,j,m,p. The detailed observation of the HRTEM images shows a nanorod morphology for pure CIS NPs (Figure 5a), for S2 (Figure 5d), and for S4 (Figure 5j). In the case of the remaining samples, S3 (Figure 5g), S5 (Figure 5m), and S6 (Figure 5p), the morphology changes to platelets. The HRTEM observation substantiates the observations of HRSEM.

The SAED patterns of pure CIS S1 (Figure 5b), S2 (Figure 5e), and S4 (Figure 5k) samples showed diffused ring patterns along with subtle spots. These observations clearly indicate the poor crystallinity of the respective samples. Samples S3 (Figure 5h), S5 (Figure 5n), and S6 (Figure 5q) show distinctive spot patterns. This observation clearly indicates the good crystallinity of samples S3, S5, and S6. The good crystallinity may be due to the morphological change from nanorods to sorted nanoplatelets due to the mediation of natural extracts. The SAED observation supports the observations of HRSEM and HRTEM.

The lattice fringe pattern of all the synthesized samples shown in Figure 5c,f,i,l,o,r clearly states the d spacing to be 0.32 nm. These d spacing values match with the value of the XRD major peak (112). This lattice fringe pattern observation clearly corroborates the XRD observation.

The overall inference derived from the morphological and SAED studies states that the basil, aloe, and turmeric mediation during synthesis modulates the morphology of the NPs and improves the crystallinity compared to that with neem and coconut. The morphology changes from nanorods to sorted nanoplates. The contents of the natural extract of basil, aloe, and turmeric help in morphology variation and hence crystallinity improvement.

2.5. Thermal Stability. The recorded TG curves for all the samples, S1, S2, S3, S4, S5, and S6, are shown in Figure 6. The TG curves are recorded for a heating rate of 10 K·min^{-1} and are recorded in an inert N_2 atmosphere over the temperature range from ambient temperature to 1253 K.

The TG curves show a continuous weight loss all through the measured temperature range. The magnitudes of weight loss for the samples are tabulated in Table 3.

The weight loss percentage observed for all the NPs lies between nearly 18% and less than a little 23%. The magnitude of the weight loss percentage states that the mediation with natural extracts has a minor effect on the thermal stability.

2.6. Optical Spectroscopy. The absorption spectra of the synthesized NPs recorded in the spectral wavelength range of 400−900 nm are shown in Figure 7.

The absorption spectra show strong absorption in the wavelength range of 408−516 nm. The absorption edges for samples S1, S2, S3, S4, S5, and S6 are 509, 441, 449, 430, 434, and 439 nm, respectively. This observation shows a significant blue shift compared to that of the bulk CIS sample (810 nm).[61,62] The reason for the blue shift in the case of synthesized NPs compared to that of bulk CIS arises due to the size effect.

The optical energy band gap (E_g) values of the synthesized NPs are evaluated by Tauc's relation[63,64]

$$(\alpha h\nu)^2 = A(h\nu - E_g) \quad (2)$$

where α, A, h, ν, and E_g denote the absorption edge coefficient, a constant related to optical transition, Planck's constant, the frequency of incident light, and the optical energy band gap, respectively.

The absorption edge coefficient (α) is calculated by the relation

$$\alpha = \frac{(B\rho)}{(MCl)} \quad (3)$$

https://doi.org/10.1021/acsomega.1c03795
ACS Omega 2021, 6, 26533−26544

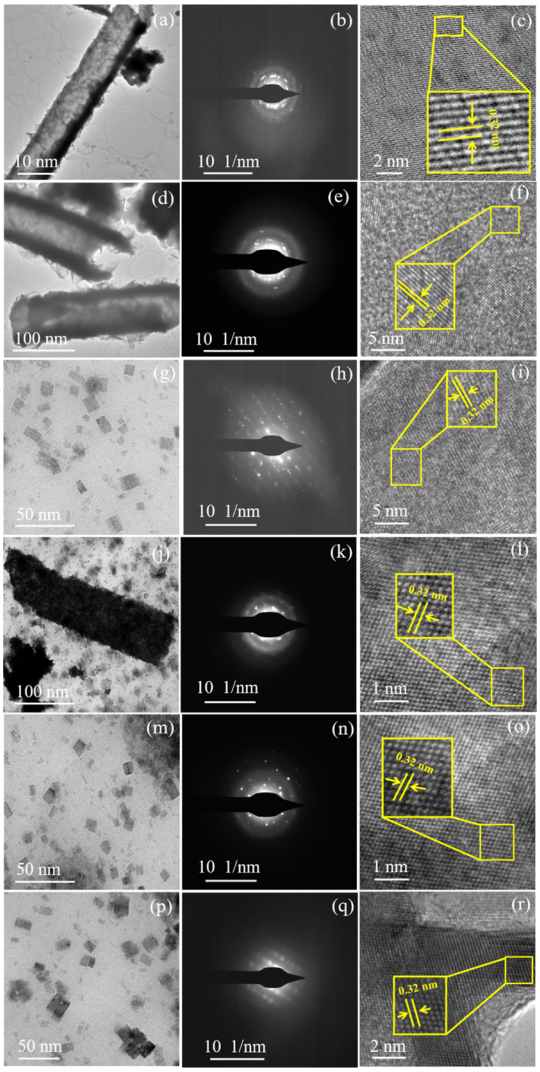

Figure 5. HRTEM images, SAED patterns, and lattice fringes of (a–c) S1; (d–f) (S2); (g–i) S3; (j–l) S4; (m–o) S5; and (p–r) S6.

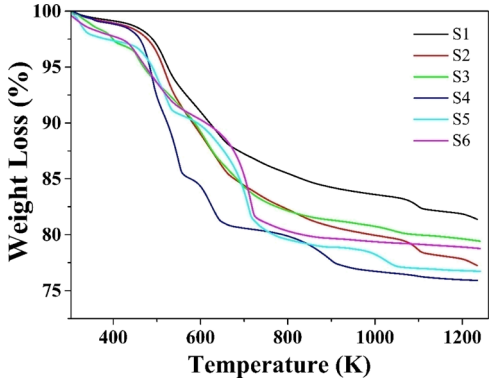

Figure 6. TG curves of S1, S2, S3, S4, S5, and S6 samples.

Here, B, ρ, M, C, and l denote the light absorbance through the sample, density of the bulk CIS sample (4.75 g·cm^{-3}),[65] molecular weight of CIS, sample concentration in the dispersing medium (acetone), and path length of light, respectively.

The plots of $(\alpha h\nu)^2$ versus $h\nu$ (Tauc's plots) for the synthesized NPs are shown in Figure 8. The extrapolation of

Table 3. Observed TG Weight Loss in the Samples

samples	weight loss (%)
S1	17.96
S2	21.38
S3	19.83
S4	22.72
S5	22.28
S6	20.36

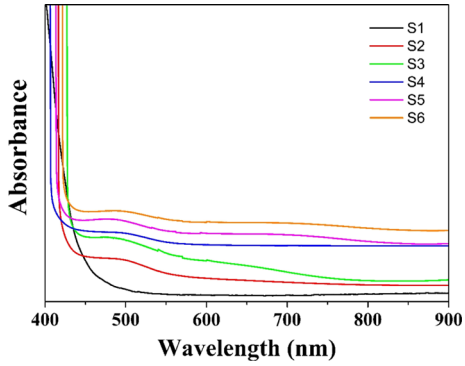

Figure 7. Absorption spectra of S1, S2, S3, S4, S5, and S6 samples.

Tauc's plots to $(\alpha h\nu)^2 = 0$ provides the best linear approximation to evaluate E_g. Table 4 shows the obtained E_g values of the synthesized NPs.

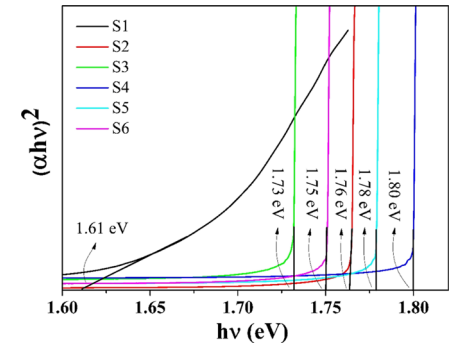

Figure 8. $(\alpha h\nu)^2$ vs $h\nu$ plots for S1, S2, S3, S4, S5, and S6 samples.

Table 4. Optical Energy Band Gap E_g Values of Synthesized NPs

samples	optical energy band gap (E_g) in eV
S1	1.61
S2	1.76
S3	1.73
S4	1.80
S5	1.78
S6	1.75

The reported optical energy band gap of the bulk CIS sample is nearly 1.55 eV.[66] The evaluated E_g values of the synthesized NPs (S1, S2, S3, S4, S5, and S6), as listed in Table 4, show blue shifts of around 0.06, 0.21, 0.18, 0.25, 0.23, and 0.20 eV, respectively, compared to that of the bulk CIS sample. The blue shift observed in the synthesized NPs confirms the quantum size effect due to the finite size of particles.

https://doi.org/10.1021/acsomega.1c03795
ACS Omega 2021, 6, 26533−26544

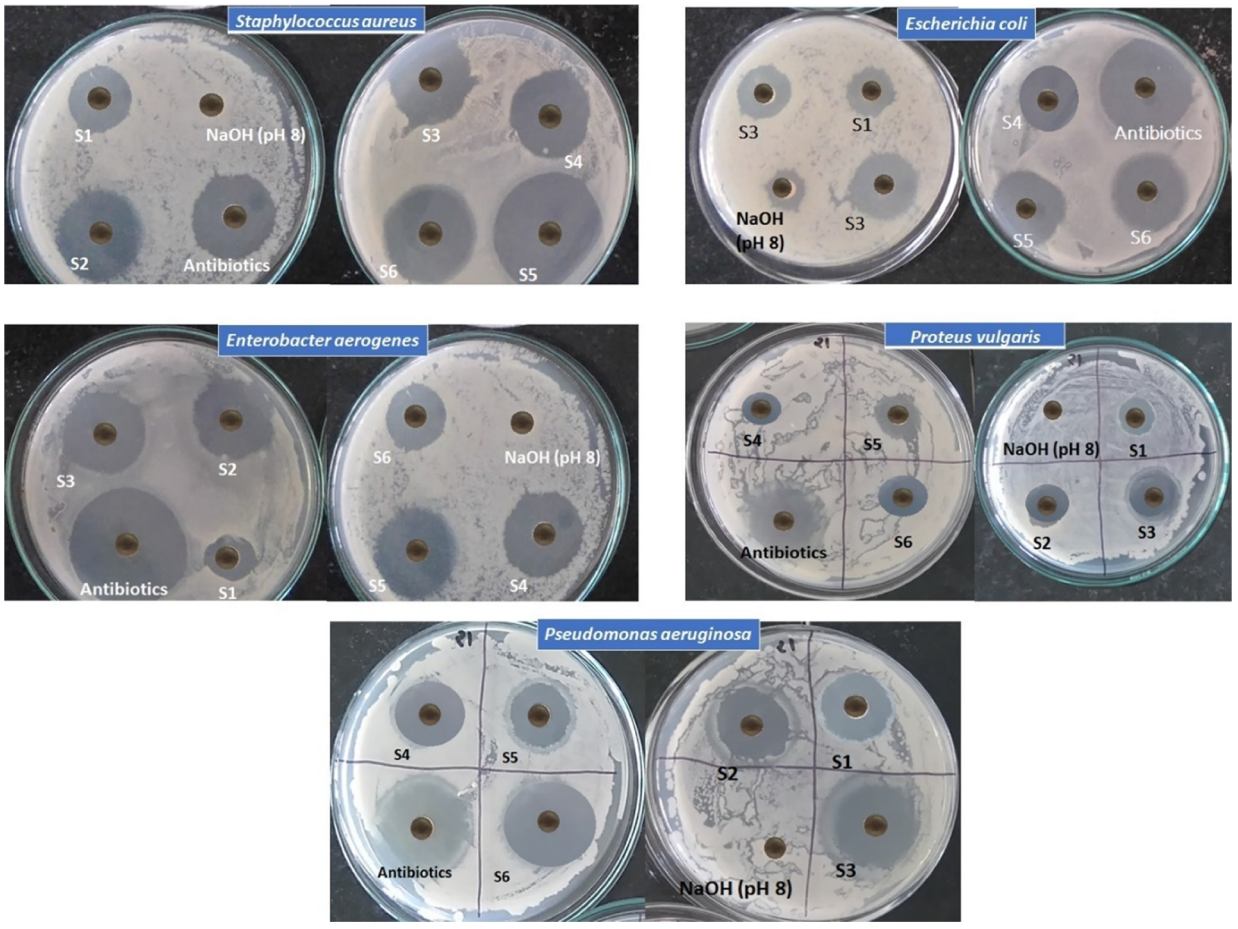

Figure 9. Antimicrobial activity of the CIS NPs.

Table 5. Values of the Zone of Inhibition and Calculated % Activity Index of the Synthesized NPs

	S. aureus		*P. aeruginosa*		*P. vulgaris*		*E. aerogenes*		*E. coli*	
samples	zone of inhibition (mm)	% activity index	zone of inhibition (mm)	% activity index	zone of inhibition (mm)	% activity index	zone of inhibition (mm)	% activity index	zone of inhibition (mm)	% activity index
S1	8	57	8	36	1	13	4	18	7	41
S2	12	86	16	73	5	63	14	64	10	59
S3	13	93	18	82	3	38	16	73	14	82
S4	13	93	9	41	2	25	16	73	11	65
S5	14	100	21	95	2	25	20	91	12	71
S6	13	93	19	86	3	38	14	64	12	71
antibiotic	14	100	22	100	8	100	22	100	17	100

3. APPLICATIONS

To validate the efficacy of the synthesized NPs in various biological fields, their antimicrobial, antioxidant, and in vivo and in vitro cytotoxicity activities are investigated.

3.1. Antimicrobial Activity. *3.1.1. Indicator Bacteria.* The plant and food-borne pathogens used for the present study are obtained from the Microbial Type Culture Collection, Chandigarh, India, to explore the antagonistic pattern of the isolates. The pathogens are *Escherichia coli* (MTCC 10312) (Gram-negative bacteria), *Pseudomonas aeruginosa* (MTCC 8076) (Gram-negative bacteria), *Proteus vulgaris* (MTCC 426) (Gram-negative bacteria), *Enterobacter aerogenes* (MTCC 111) (Gram-negative bacteria), and *Staphylococcus aureus* (MTCC 9542) (Gram-positive bacteria).

3.1.2. Antagonistic Activity against Indicator Microbes. The antagonistic activity studies of the synthesized NPs are performed by the agar-well diffusion (Thornton 1996) technique against mastitis-causing pathogens. A volume of 1 mL of the inoculum of each indicator organism (conc. 1×10^6 cell/mL) is added to slightly warm nutrient agar. It is mixed well, then poured into Petri plates separately, and allowed to solidify. Wells 9 mm in diameter are cut, and 50 μL of NP suspension prepared in 10% dimethyl sulfoxide (DMSO) (25 mg/mL) is poured into each well separately. The plates are incubated for 30 min at 288 K for the uniform diffusion of the supernatant and later maintained at 310 K for 24 h. Clear zones formed around the wells are measured (Figure 9). The same protocol is carried out for the same concentration of standard antibacterial antibiotic ampicillin using the same

https://doi.org/10.1021/acsomega.1c03795
ACS Omega 2021, 6, 26533−26544

solvent for finding the percent activity index. The formula used is as follows

$$\%\ \text{activity index} = [\text{zone of inhibition using CIS nanoparticles (diameter in mm)}] / [\text{zone of inhibition using standard antibiotic (diameter in mm)}] \times 100 \quad (4)$$

3.1.3. Minimum Inhibitory Concentration. Six different concentrations of the CIS NPs ranging from 10 to 0.3 mg/mL are prepared in nutrient broth, separately. All indicator bacterial inocula are prepared by adjusting the turbidity equivalent to 0.5 McFarland turbidity standard. A 50 μL volume of the prepared inoculum is added to 1 mL of modified N-broth and mixed. Tubes are sealed and incubated at 310 K for 24 h. The minimum inhibitory concentration (MIC) is determined by selecting the lowest concentration of NPs, which completely inhibits the growth in the tube, as detected by the unaided eye and by considering the optical density at 620 nm. The observed MIC values for the synthesized CIS NPs are tabulated in Table 6.

Table 6. MIC Values of the CIS NPs

	MIC values (mg/mL)				
samples	*S. aureus*	*P. aeruginosa*	*P. vulgaris*	*E. aerogenes*	*E. coli*
S1	1.250	2.500	10.000	2.500	1.250
S2	0.625	1.250	1.250	1.250	1.250
S3	0.625	1.250	2.500	0.625	0.300
S4	0.625	2.500	5.000	0.625	0.625
S5	0.300	0.300	5.000	0.300	0.625
S6	0.625	0.625	2.500	1.250	0.625

Dose-dependent inhibitory effects of the microbial growth for synthesized S1, S2, S3, S4, S5, and S6 CIS NPs against indicator bacterial isolates are explored using the broth microdilution technique.

3.2. Antioxidant Activity. The antioxidant activity of the synthesized NPs is investigated by employing the simplest and rapid approach using a 2,2-diphenyl-1-picrylhydrazyl (DPPH) assay. The DPPH assay contains a nitrogen-centered stable radical deep-violet in color having a maximum absorption peak at 517 nm. The antioxidant activity of synthesized NPs is evaluated using the as-reported method by Das et al. (2013).[67] The DPPH scavenging assay is used to explore the scavenging potential of antioxidants, that is, NPs against stable radicals. The radical scavenging assay is measured by a UV spectrophotometer at 517 nm. An aliquot of each synthesized NP and vitamin C as a standard are mixed with 1 mL of freshly prepared methanol DPPH solution (1 mM) with different concentrations ranging from 12.5 to 400 μg/mL; afterward, each tube containing the mixture is incubated in the dark for 30 min, and the absorbance at 517 nm is obtained. Here, methanol is taken as a blank. IC_{50} is explained as the concentration (μg/mL) that shows 50% inhibition of the DPPH activity by reducing the color of it in the presence of an antioxidant against synthesized NPs. The calculation is performed using the equation

$$IC_{50}(\%) = 100 \times \frac{(A_0 - A_s)}{A_0} \quad (5)$$

Here, A_s and A_0 are the absorbance values of the sample and the negative control, respectively.

The activity is investigated spectrophotometrically by observing the change in color from deep violet to pale yellow. The observed % radical scavenging activity values at different concentrations of the control (vitamin C) for the samples are tabulated in Table 7. The percentage of the radical scavenging activity of the samples is found to increase with the increase in the concentration of the samples.

Table 7. % Radical Scavenging Activity Values of Vitamin C (Control) and Those of the Synthesized NPs at Various Concentrations

	% radical scavenging activity concentration (μg/mL)				
samples	12.5	25	50	100	IC_{50} value (μg/mL)
vitamin C (control)	22	31	37	44	91.0
S1	27	33	39	45	87.2
S2	28	35	40	46	84.9
S3	28	38	42	47	82.0
S4	26	33	39	47	85.1
S5	37	44	48	50	74.1
S6	24	36	41	53	85.7

3.3. In Vivo Cytotoxicity Study (Brine Shrimp Lethality Test). To investigate the in vivo cytotoxicity, (*Artemia salina*) eggs are hatched in artificial seawater prepared from commercial sea salt (38 g/L). A lamp is placed above the open side of the tank to attract the hatched shrimps close to the tank wall. After 24 h, the shrimps are matured as nauplii (*A. salina*) and are ready for the assay. The brine shrimp lethality bioassay is carried out for the synthesized NPs using the standard procedure. All NPs (25 mg) are dissolved in 1 mL of 1 M NaOH (pH 8.0) to obtain a concentration of 25 mg/mL. A Petri plate containing 1 M NaOH (pH 8.0) in 5 mL of saltwater is used as the negative control. Potassium dichromate (as the positive control) is dissolved in 1 M NaOH (pH 8.0) and serially diluted to a concentration of 5 mg/mL. 0.1 mL of a suspension of larvae, which contains about 10 larvae, is added to each Petri plate and incubated for 24 h. The Petri plates are examined carefully, and the number of dead larvae in each bottle is counted after 24 h. The death percentage of shrimp is calculated using the equation

$$\%\ \text{mortality} = \frac{\text{total shrimp} - \text{alive shrimp}}{\text{total shrimp}} \times 100 \quad (6)$$

LC_{50} is explained as the concentration (μg/mL) that kills 50% of the shrimp, obtained using the lethality assay. The evaluated mortality rate of shrimp and LC_{50} values for the synthesized NPs are tabulated in Table 8. Figure 10 exhibits a bar graph showing the maximum % mortality of shrimp and LC_{50} values for the synthesized NPs.

3.4. In Vitro Cytotoxicity Study (Antiproliferative Test). To investigate the in vitro cytotoxicity study, the as-synthesized CIS NPs are dissolved in DMSO (Sigma-Aldrich, St. Louis, MO, USA; cat no. D8418-500ML) and further diluted with a culture medium to the desired concentration. The compound solutions are freshly prepared before use. Human lung carcinoma cell lines (A549) are procured from NCCS, Pune, India. The cell line is maintained as a monolayer in Dulbecco's modified Eagle medium/nutrient mixture F12 (Gibco, Invitrogen, CA, USA; cat no. 11320033) containing

https://doi.org/10.1021/acsomega.1c03795
ACS Omega 2021, 6, 26533−26544

Table 8. Evaluated Mortality Rate of Shrimp and LC_{50} Values for the Synthesized NPs

samples	conc. (μg/mL)	% mortality	LC_{50} (μg/mL)
S1	25	20	52.9
	50	40	
	75	70	
	100	100	
S2	25	10	70.8
	50	30	
	75	60	
	100	70	
S3	25	20	55.0
	50	40	
	75	60	
	100	100	
S4	25	10	64.7
	50	30	
	75	50	
	100	90	
S5	25	10	87.3
	50	30	
	75	40	
	100	60	
S6	25	10	61.5
	50	30	
	75	60	
	100	90	

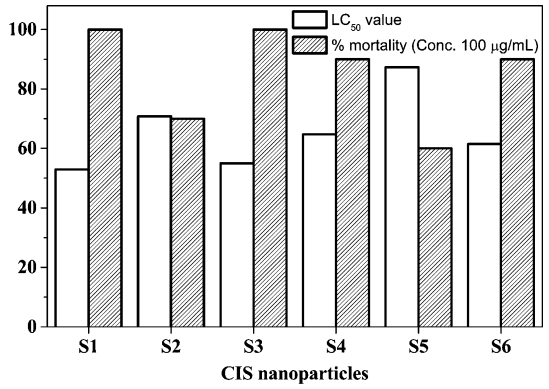

Figure 10. Maximum % mortality of shrimp and LC_{50} values for the synthesized NPs.

10% fetal bovine serum (Gibco, Invitrogen, CA, USA; cat no. 1600069) supplemented with 50 U/mL penicillin and 50 μg/mL streptomycin (Gibco, Invitrogen, CA, USA; cat no. 15140122) at 310 K in a humidified atmosphere of 5% CO_2/95% air.[68]

An antiproliferative assay in response to all NP treatments is carried out as per the method described by Gajera et al.[69] Briefly, 10,000 cells/well are seeded in 96-well culture plates and incubated for 24 h. After 24 h, the cells are treated with various concentrations of NPs to find out the appropriate IC_{50} value. The next day, 5 μL of MTT [3-(4,5-dimethylthiazol-2-yl)-2,5-diphenyltetrazolium bromide] (5 mg/mL) is added to each well and incubated for 3−4 h in a CO_2 incubator at 310 K. The volume of the culture is 100 μL in each well. After the incubation period, the removal of the culture medium is accomplished, and the obtained purple crystals are dissolved in 100 μL of molecular-grade DMSO. The absorbance is recorded at 570 nm using a microplate reader.

The IC_{50} values for the A549 cell line after 24 h of treatment with different as-synthesized NPs are given in Table 9. These values are obtained from the MTT assay for the cytotoxic potential of the samples. The values represent the mean ± standard error for the assay performed in triplicate.

Table 9. IC_{50} Values of the A549 Cell Line with the CIS NPs

samples	IC_{50} value (μg/mL)
S1	117.22 ± 2.22
S2	94.57 ± 2.92
S3	42.65 ± 1.98
S4	30.96 ± 2.88
S5	28.43 ± 2.55
S6	15.62 ± 1.58

4. RESULTS AND DISCUSSION

Table 5 reveals that the antagonistic activity of pure CIS NPs (S1) is less effective against all pathogens than that of synthesized natural extract-mediated NPs. Antibacterial broad-spectrum effects are observed in the outcomes. The results show that the synthesized natural extract aloe-mediated CIS NPs (S5) have a broad inhibitory spectrum but the best inhibitory effect is observed against *S. aureus* (Gram-positive bacteria), whereas *P. vulgaris* (Gram-negative bacteria) exhibits less sensitivity. *S. aureus* is a Gram-positive bacteria having a thick cell wall composed of peptidoglycan. Peptidoglycan is a polymer consisting of amino acids and sugars that produces a mesh-like layer outside the bacterial plasma membrane. In Gram-negative bacteria, the outer cell wall is of peptidoglycan, a monolayer. Outside this layer, there is an envelope of membrane structures. This structure is moored noncovalently to lipoprotein particles, which are covalently connected to peptidoglycan. Thus, the lipopolysaccharides (LPSs) structure some portion of the outer cell wall of Gram-negative bacteria. These LPSs elicit strong immune responses, thus leading to noninteraction with the present CIS NPs. The antimicrobial activity occurs by a mechanism in which the Cu ions of the CIS NPs complex with chelating agarose, a linear polymer of agar base. These chelated cations leave holes in the cell walls of the pathogens, leading to a complete breakdown and leaving it ineffective. The mechanism of chelating enhances the antipathogen properties of CIS. In Gram-negative bacteria, due to the presence of an additional LPS layer on peptidoglycan in the cell wall, the protection against chelating is enhanced, whereas in *S. aureus,* the cell wall is formed of peptidoglycan only, which gets chelated.

The natural extract-mediated NPs showed a larger diameter of the zone and a higher activity index than pure CIS NPs. Among all the natural extract-mediated NPs, aloe-mediated CIS NPs (S5) showed the best antimicrobial activity. The presence of anthraquinones, dihydroxyanthraquinone, saponins, and so forth in aloe leaf extracts enhances the antimicrobial activity.[70]

Table 6 shows that the least MIC values are observed in the cases of S5 CIS NPs (0.300 mg/mL) against *S. aureus*, *P. aeruginosa,* and *E. aerogenes* and the S3 CIS NPs (0.300 mg/mL) against *E. coli*.

In Table 7, the comparable percentage of the scavenging activity of the samples against the control (vitamin C) is observed. The percentage inhibition of the free radical for natural extract-mediated NPs is found to increase in a

https://doi.org/10.1021/acsomega.1c03795
ACS Omega 2021, 6, 26533−26544

concentration-dependent manner, exhibiting a minimum IC_{50} value for S5 of 74.1 μg/mL (50% inhibition), followed by that for S3 NPs of 82 μg/mL (47% inhibition), compared with the standard (vitamin C) IC_{50} value (91 μg/mL). The presence of polysaccharides and flavonoids as a specific content in the employed natural extracts is responsible for good antioxidant activity.[71−74] It can be clearly stated that to inhibit the activity, the maximum concentration for the control (vitamin C) and the minimum concentration for S5 is needed. The synthesized NPs mediated by natural extracts showed the requirement of comparable concentrations to that of the control. This observation confirms the efficacy of the synthesized NPs mediated by natural extracts.

Table 8 confirms that the increase in the mortality rate affects the LC_{50} value. The observation states that the LC_{50} value for the synthesized NP sample S1 is the lowest, 52.9 μg/mL. This may be due to the pure chemical synthesis of S1. The chemical synthesis makes the NPs toxic to microbes. The literature states that an LC_{50} value of less than 55 μg/mL represents anticancer properties[75] and an LC_{50} value of less than 1000 μg/mL represents bioactive and toxic properties.[76] In the present studies for natural extract-mediated NPs, the LC_{50} values indicate them to be toxic as well as efficiently bioactive.

From Table 9, it can be stated that out of the six samples of the synthesized NPs (S1, S2, S3, S4, S5, and S6), the NPs mediated by turmeric extracts (S6) have the lowest IC_{50} value of 15.62 μg/mL. This means that S6 is the most potent in terms of cytotoxicity toward A549. Turmeric is considered a widely studied anticancer agent, which is a prime reason for the potent activity of the CIS NPs mediated by turmeric extracts (S6). The second most potent compound is CIS NPs mediated by aloe extracts (S5) with the IC_{50} value of 28.43 μg/mL. The CIS NPs mediated by coconut water extracts (S4) also showed good efficacy in terms of cytotoxicity toward A549 cells. Pure CIS NPs (S1) have shown comparatively poor cytotoxicity among all the six studied samples.

5. CONCLUSIONS

The pure CIS NPs and natural extract-mediated CIS NPs are synthesized by the hydrothermal route. The natural extracts used for the mediation in the CIS NP synthesis are *A. indica* (neem), *O. sanctum* (basil), *C. nucifera* (coconut), *A. vera* (aloe), and *C. longa* (turmeric). The XRD analysis showed that all the NPs possesses a tetragonal unit cell structure with the lattice parameters $a = b = 5.51$ Å, $c = 11.32$ Å, and $\alpha = \beta = \gamma = 90°$. The average crystallite size of pure CIS NPs is maximum and that of NPs mediated by coconut water extracts is minimum. The EDAX analysis shows that all the NPs are near-stoichiometric. The morphology study by HRSEM and HRTEM showed pure CIS NPs to have a nanorod shape. The neem and coconut extract mediation does not change the nanorod shape, whereas the other natural extract mediation changes the shape from nanorods to sorted nanoplates. The SAED study showed that the mediation of natural extracts of basil, aloe, and turmeric helps in crystallinity improvement. The TG study of the synthesized NPs showed them to possess a weight loss between ∼18% and a little less than 23%. The optical band gap study showed a blue shift in the absorption edge of all the samples compared to the bulk CIS band gap value. The blue shift arises due to size confinement. From the antimicrobial activity, a broad inhibitory spectrum is observed for the aloe-mediated CIS NPs. The best inhibitory effect is observed against *S. aureus,* whereas *P. vulgaris* exhibited the least effect. S5 (aloe) CIS NPs show the least MIC value (0.300 mg/mL) against *S. aureus*, *P. aeruginosa* and *E. aerogenes*, along with S3 (basil) against *E. coli*. From the antioxidant activity, the IC_{50} value to inhibit the scavenging activity is found to be the maximum for the control (vitamin C) and the minimum for pure CIS NPs (S1). The in vivo cytotoxicity study using brine shrimp eggs shows that the pure CIS NPs (S1) are more lethal to brine shrimp than the natural extract-mediated CIS NPs. The in vitro cytotoxicity study using the human lung carcinoma cell line (A549) confirms the high potency and efficacy for the natural extract-mediated CIS NPs compared to that of pure CIS NPs. The IC_{50} value of the A549 cell line with turmeric extract-mediated CIS NPs is the minimum. This observation reveals that turmeric extract-mediated CIS NPs are the most potent in terms of cytotoxicity toward the A549 cell line.

The current findings in this research article set a benchmark and open up a new approach to synthesize biocompatible metal chalcogenide semiconductors with lower cytotoxicity that can be employed in various biological applications including bioimaging, biosensing, targeted drug delivery, fluorescent biological labeling, protein detection, tissue engineering, and so forth more safely and efficiently than traditional approaches.

6. EXPERIMENTAL SECTION

6.1. Plant Material. In the present study, the leaves of *A. indica* (neem), *O. sanctum* (basil), and *A. vera* (aloe) are collected from our own university campus in January 2021. *C. nucifera* (coconut) fruit and *C. longa* (turmeric) organic powder are purchased from the local market.

6.2. Extraction. The collected neem, basil, and aloe leaves are thoroughly washed with double-distilled water. Leaves weighing 10 g are allowed to dry under shade at room temperature. The green skin of aloe leaves is peeled off, and the gel is removed. Each of the leaves is finely chopped into smaller pieces. These finely chopped pieces are mixed in 50 mL of double-distilled water. The mixture is boiled for 20 min at 353 K under constant stirring and allowed to cool down to room temperature. The resultant extract is filtered using a Grade-5 Whatman filter paper and centrifuged at 3000 rpm for 30 min to remove the sediments. In the case of coconut water, the extract is collected in a clean glass beaker by drilling a hole in a fresh raw coconut. The extracted coconut water is filtered using a Grade-5 Whatman filter paper before use in NP synthesis. The extraction process of turmeric powder is quite similar to that of leaves. In this case, 3.4 g of organic turmeric powder is dissolved in 50 mL of double-distilled water by magnetic stirring, as suggested by Alsammarraie et al.[77] The mixture is boiled for 20 min and allowed to cool down to room temperature. The extract is filtered and centrifuged at 3000 rpm for 30 min. All the above filtrates are stored at 277 K before use in synthesis.

6.3. Synthesis of CIS NPs. *6.3.1. Chemicals Used.* The synthesis of CIS NPs is done using cupric chloride dihydrate ($CuCl_2·2H_2O$) [minimum assay 98%, Astron Chemicals, India], indium(III) chloride tetrahydrate ($InCl_3·4H_2O$) [minimum assay 99.99%, Sisco Research Laboratories (SRL) Pvt. Ltd., India], thioacetamide (C_2H_5NS) [minimum assay 99%, Sisco Research Laboratories (SRL) Pvt. Ltd., India], and Triton X-100 [minimum hydroxyl value 85%, HiMedia

https://doi.org/10.1021/acsomega.1c03795
ACS Omega 2021, 6, 26533−26544

Laboratories Pvt. Ltd., Mumbai, India]. All chemicals are used without any processing or purification.

6.3.2. Green Synthesis Technique. The CIS NPs are synthesized by a hydrothermal route. Initially, 10.23 g of $CuCl_2$ $2H_2O$ is dissolved in 300 mL of double-distilled water to prepare a 0.2 M precursor solution. Simultaneously, 17.59 g of $InCl_3$ $4H_2O$ is dissolved in 300 mL of double-distilled water to prepare another 0.2 M precursor solution. Both the precursor solutions are mixed by magnetic stirring for 30 min. To the above mixture, 300 mL of 0.6 M C_2H_5NS (13.52 g) is added. The mixture is stirred for 30 min. After that, a 0.5 mM (5.6 mL) Triton X-100 surfactant is added. The solution is thoroughly stirred, leading to proper mixing. The above prepared solution is further divided into six equal parts in six glass beakers.

The first beaker is kept as it is without any processing, denoting pure CIS NPs, and labeled as S1. In the other five beakers containing the solution, the prepared extracts of the neem leaf, basil leaf, coconut water, aloe leaf, and turmeric powder are added separately, which in turn provides CIS NPs mediated by extracts of the neem leaf (S2), basil leaf (S3), coconut water (S4), aloe leaf (S5), and turmeric powder (S6).

Ultimately, each prepared solution is loaded into a vertical autoclave (double-wall, stainless-steel-based, pressure range: 10−12 bar, voltage: 230 V, frequency: 50−60 Hz, power: 2 kW) and heated to 383 K for 12 h. The final solution becomes blackish-brown in color. The precipitates are filtered using a Grade-5 filter paper. The NP yields are given multiple double-distilled water wash to remove impurities. The NPs are dried in a hot-air oven for 10 h at 318 K.

AUTHOR INFORMATION

Corresponding Authors

Ranjan Kr. Giri − *P. G. Department of Physics, Sardar Patel University, Vallabh Vidyanagar 388120 Gujarat, India;* orcid.org/0000-0002-9702-1566; Email: ranjankrgiri@gmail.com

Sunil Chaki − *P. G. Department of Physics, Sardar Patel University, Vallabh Vidyanagar 388120 Gujarat, India; Department of Applied & Interdisciplinary Sciences, CISST, Sardar Patel University, Vallabh Vidyanagar 388120 Gujarat, India*; Email: sunilchaki@yahoo.co.in

Authors

Ankurkumar J. Khimani − *Department of Physics, Shri A. N. Patel P. G. Institute of Science and Research, Anand 388001 Gujarat, India*

Yati H. Vaidya − *Department of Microbiology, Shri A. N. Patel P. G. Institute of Science and Research, Anand 388001 Gujarat, India*

Parth Thakor − *P. G. Department of Biosciences, Sardar Patel University, Bakrol 388315 Gujarat, India*

Anjali B. Thakkar − *Department of Applied & Interdisciplinary Sciences, CISST, Sardar Patel University, Vallabh Vidyanagar 388120 Gujarat, India; P. G. Department of Biosciences, Sardar Patel University, Bakrol 388315 Gujarat, India*

Swati J. Pandya − *P. G. Department of Physics, Sardar Patel University, Vallabh Vidyanagar 388120 Gujarat, India*

Milind P. Deshpande − *P. G. Department of Physics, Sardar Patel University, Vallabh Vidyanagar 388120 Gujarat, India*

Complete contact information is available at: https://pubs.acs.org/10.1021/acsomega.1c03795

Notes

The authors declare no competing financial interest.

ACKNOWLEDGMENTS

One of the authors, R.K.G., is thankful to the Education Department, Government of Gujarat, India, for providing the Research Fellowship under SHODH (ScHeme Of Developing High quality research, grant no. 201901640031) to carry out the research work.

REFERENCES

(1) Heidariramsheh, M.; Dabbagh, M. M.; Mahdavi, S. M.; Beitollahi, A. Morphology and Phase-Controlled Growth of $CuInS_2$ Nanoparticles through Polyol Based Heating up Synthesis Approach. *Mater. Sci. Semicond. Process.* **2021**, *121*, 105401.

(2) Ning, J.; Kershaw, S. V.; Rogach, A. L. Shape-Controlled Synthesis of Copper Indium Sulfide Nanostructures: Flowers, Platelets and Spheres. *Nanomaterials* **2019**, *9*, 1779.

(3) Kharkwal, A.; Sharma, S. N.; Jain, K.; Singh, A. K. A Solvothermal Approach for the Size-, Shape- and Phase-Controlled Synthesis and Properties of $CuInS_2$. *Mater. Chem. Phys.* **2014**, *144*, 252−262.

(4) Li, F.; Tao, R.; Cao, B.; Yang, L.; Wang, Z. Manipulate the Light-Matter Interaction of PtS/MoS_2 p−n Junction for High Performance Broadband Photodetection. *Adv. Funct. Mater.* **2021**, *31*, 2104367.

(5) Zhang, Y.; Tian, J.; Li, H.; Wang, L.; Qin, X.; Asiri, A. M.; Al-Youbi, A. O.; Sun, X. Biomolecule-Assisted, Environmentally Friendly, One-Pot Synthesis of CuS/Reduced Graphene Oxide Nanocomposites with Enhanced Photocatalytic Performance. *Langmuir* **2012**, *28*, 12893−12900.

(6) Liu, Q.; Xie, L.; Liu, Z.; Du, G.; Asiri, A. M.; Sun, X. A Zn-Doped Ni_3S_2 Nanosheet Array as a High-Performance Electrochemical Water Oxidation Catalyst in Alkaline Solution. *Chem. Commun.* **2017**, *53*, 12446−12449.

(7) Zhao, W.; Wang, X.; Ma, X.; Yue, L.; Liu, Q.; Luo, Y.; Liu, Y.; Asiri, A. M.; Sun, X. In Situ Tailoring Bimetallic−Organic Framework-Derived Yolk−Shell NiS_2/CuS Hollow Microspheres: An Extraordinary Kinetically Pseudocapacitive Nanoreactor for an Effective Sodium-Ion Storage Anode. *J. Mater. Chem. A* **2021**, *9*, 15807−15819.

(8) Zhao, W.; Gao, L.; Yue, L.; Wang, X.; Liu, Q.; Luo, Y.; Li, T.; Shi, X.; Asiri, A. M.; Sun, X. Constructing a Hollow Microflower-like ZnS/CuS@C Heterojunction as an Effective Ion-Transport Booster for an Ultrastable and High-Rate Sodium Storage Anode. *J. Mater. Chem. A* **2021**, *9*, 6402−6412.

(9) Li, S.; Wu, Y.; Liu, Q.; Li, B.; Li, T.; Zhao, H.; Alshehri, A. A.; Alzahrani, K. A.; Luo, Y.; Li, L.; Sun, X. CuS Concave Polyhedral Superstructures Enabled Efficient N_2 Electroreduction to NH_3 at Ambient Conditions. *Inorg. Chem. Front.* **2021**, *8*, 3105−3110.

(10) Goto, M.; Sato, K.; Yokoyama, S.; Takahashi, H. One-Step Synthesis of $CuInS_2$ Nanoparticles Using Aqueous Chelated Metal Complexes as a Starting Material. *J. Mater. Sci.: Mater. Electron.* **2021**, *32*, 9531−9539.

(11) Takahashi, H.; Goto, M.; Yokoyama, S. Water Phase Synthesis Method of $CuInS_2$ Nanoparticles and Its Application for Photovoltaic Device. *ECS Meet. Abstr.* **2020**, *2020-0*, 1444.

(12) Cheshme Khavar, A. H.; Mahjoub, A. R.; Tajabadi, F.; Dehghani, M.; Taghavinia, N. Preparation of a $CuInS_2$ Nanoparticle Ink and Application in a Selenization-Free, Solution-Processed Superstrate Solar Cell. *Eur. J. Inorg. Chem.* **2015**, 5793−5800.

(13) Long, Z.; Zhang, W.; Tian, J.; Chen, G.; Liu, Y.; Liu, R. Recent Research on the Luminous Mechanism, Synthetic Strategies, and Applications of $CuInS_2$ Quantum Dots. *Inorg. Chem. Front.* **2021**, *8*, 880−897.

(14) Li, J.; Jin, H.; Wang, K.; Xie, D.; Xu, D.; Xu, X.; Xu, G. High Luminance of $CuInS_2$-Based Yellow Quantum Dot Light Emitting Diodes Fabricated by All-Solution Processing. *RSC Adv.* **2016**, *6*, 72462−72470.

(15) Hou, H.; Yuan, Y.; Cao, S.; Yang, Y.; Ye, X.; Yang, W. $CuInS_2$ Nanoparticles Embedded in Mesoporous TiO_2 Nanofibers for Boosted Photocatalytic Hydrogen Production. *J. Mater. Chem. C* **2020**, *8*, 11001−11007.
(16) Chumha, N.; Pudkon, W.; Chachvalvutikul, A.; Luangwanta, T.; Randorn, C.; Inceesungvorn, B.; Ngamjarurojana, A.; Kaowphong, S. Photocatalytic Activity of $CuInS_2$ Nanoparticles Synthesized via a Simple and Rapid Microwave Heating Process. *Mater. Res. Express* **2020**, *7*, 015074.
(17) Arshad, A.; Akram, R.; Iqbal, S.; Batool, F.; Iqbal, B.; Khalid, B.; Khan, A. U. Aqueous Synthesis of Tunable Fluorescent, Semiconductor $CuInS_2$ Quantum Dots for Bioimaging. *Arabian J. Chem.* **2019**, *12*, 4840−4847.
(18) Chetty, S. S.; Praneetha, S.; Basu, S.; Sachidanandan, C.; Murugan, A. V. Sustainable, Rapid Synthesis of Bright-Luminescent $CuInS_2$-ZnS Alloyed Nanocrystals: Multistage Nano-Xenotoxicity Assessment and Intravital Fluorescence Bioimaging in Zebrafish-Embryos. *Sci. Rep.* **2016**, *6*, 26078.
(19) Bhatt, V. K.; Patel, M.; Pataniya, P. M.; Iyer, B. D.; Sumesh, C. K.; Late, D. J. Enhanced Antifungal Activity of WS_2/ZnO Nanohybrid against Candida Albicans. *ACS Biomater. Sci. Eng.* **2020**, *6*, 6069−6075.
(20) Chang, W.-G.; Tao, L.-L. Hydrothermal Synthesis and Optical Properties of $CuInS_2$ Micro-/Nanomaterials by Using Gemini Surfactant as Soft Template. *J. Appl. Spectrosc.* **2019**, *86*, 549−553.
(21) Lee, J.; Han, C.-S. Bright, Stable, and Water-Soluble $CuInS_2$/ZnS Nanocrystals Passivated by Cetyltrimethylammonium Bromide. *Nanoscale Res. Lett.* **2015**, *10*, 145.
(22) Piber, M.; Rath, T.; Griesser, T.; Trimmel, G.; Stelzer, F.; Meissner, D. Hybrid Solar Cells Based on $CuInS_2$ and MEH-PPV. In *2006 IEEE 4th World Conference on Photovoltaic Energy Conference*, 2006; Vol. *1*, pp 247−248.
(23) Bu, H.-B.; Yokota, H.; Shimura, K.; Takahasi, K.; Taniguchi, T.; Kim, D. Hydrothermal Synthesis of N-Acetyl-L-Cysteine-Capped $CuInS_2$ Nanoparticles. *Chem. Lett.* **2015**, *44*, 200−202.
(24) Lefrançois, A.; Pouget, S.; Vaure, L.; Lopez-Haro, M.; Reiss, P. Direct Synthesis of Highly Conductive Tert-Butylthiol-Capped $CuInS_2$ Nanocrystals. *ChemPhysChem* **2016**, *17*, 654−659.
(25) Asgary, S.; Mirabbaszadeh, K.; Nayebi, P.; Emadi, H. Synthesis and Investigation of Optical Properties of TOPO-Capped $CuInS_2$ Semiconductor Nanocrystal in the Presence of Different Solvent. *Mater. Res. Bull.* **2014**, *51*, 411−417.
(26) Dutková, E.; Bujňáková, Z. L.; Kello, M.; Mojžiš, J.; Skurikhina, O.; Briančin, J. Chitosan Capped $CuInS_2$ and $CuInS_2$/ZnS by Wet Stirred Media Milling: In Vitro Verification of Their Potential Bio-Imaging Applications. *Appl. Nanosci.* **2020**, *10*, 4661−4671.
(27) Lee, J.; Han, C.-S. Large-Scale Synthesis of Highly Emissive and Photostable $CuInS_2$/ZnS Nanocrystals through Hybrid Flow Reactor. *Nanoscale Res. Lett.* **2014**, *9*, 78.
(28) Yu, C.; Xuan, T.; Lou, S.; Liu, X.; Lian, G.; Li, H. Gd^{3+} Doped $CuInS_2$/ZnS Nanocrystals with High Quantum Yield for Bimodal Fluorescence/Magnetic Resonance Imaging. *J. Rare Earths* **2017**, *35*, 382−388.
(29) Handago, D. T.; Zereffa, E. A.; Gonfa, B. A. Effects of Azadirachta Indica Leaf Extract, Capping Agents, on the Synthesis of Pure And Cu Doped ZnO-Nanoparticles: A Green Approach and Microbial Activity. *Open Chem.* **2019**, *17*, 246−253.
(30) Thirumurugan, A.; Aswitha, P.; Kiruthika, C.; Nagarajan, S.; Christy, A. N. Green Synthesis of Platinum Nanoparticles Using Azadirachta Indica − An Eco-Friendly Approach. *Mater. Lett.* **2016**, *170*, 175−178.
(31) Lee, S. Y.; Krishnamurthy, S.; Cho, C.-W.; Yun, Y.-S. Biosynthesis of Gold Nanoparticles Using Ocimum Sanctum Extracts by Solvents with Different Polarity. *ACS Sustainable Chem. Eng.* **2016**, *4*, 2651−2659.
(32) Ramteke, C.; Chakrabarti, T.; Sarangi, B. K.; Pandey, R.-A. Synthesis of Silver Nanoparticles from the Aqueous Extract of Leaves of Ocimum Sanctum for Enhanced Antibacterial Activity. *J. Chem.* **2013**, *2013*, 278925.
(33) Rajesh, M. K.; Muralikrishna, K. S.; Nair, S. S.; Kumar, B. K.; Subrahmanya, T. M.; Sonu, K. P.; Subaharan, K.; Sweta, H.; Prasad, T. S. K.; Chandran, N.; Hebbar, K. B.; Karun, A. Coconut Inflorescence Sap Mediated Synthesis of Silver Nanoparticles and Its Diverse Antimicrobial Properties. **2009**, bioRxiv:10.1101/775940.
(34) Fardsadegh, B.; Jafarizadeh-Malmiri, H. Aloe Vera Leaf Extract Mediated Green Synthesis of Selenium Nanoparticles and Assessment of Their In Vitro Antimicrobial Activity against Spoilage Fungi and Pathogenic Bacteria Strains. *Green Process. Synth.* **2019**, *8*, 399−407.
(35) Bhattacharya, G.; Sas, S.; Wadhwa, S.; Mathur, A.; McLaughlin, J.; Roy, S. S. Aloe Vera Assisted Facile Green Synthesis of Reduced Graphene Oxide for Electrochemical and Dye Removal Applications. *RSC Adv.* **2017**, *7*, 26680−26688.
(36) Sharma, M.; Monika; Thakur, P.; Saini, R. V.; Kumar, R.; Torino, E. Unveiling Antimicrobial and Anticancerous Behavior of Au NPs and Ag NPs Moderated by Rhizome Extracts of Curcuma Longa from Diverse Altitudes of Himalaya. *Sci. Rep.* **2020**, *10*, 10934.
(37) Alzohairy, M. A. Therapeutics Role of Azadirachta Indica (Neem) and Their Active Constituents in Diseases Prevention and Treatment. *J. Evidence-Based Complementary Altern. Med.* **2016**, *2016*, 7382506.
(38) Kaya, I.; Yigit, N.; Benli, M. Antimicrobial Activity of Various Extracts of Ocimum Basilicum L. and Observation of the Inhibition Effect on Bacterial Cells by Use of Scanning Electron Microscopy. *Afr. J. Tradit., Complementary Altern. Med.* **2008**, *5*, 363−369.
(39) Satheshkumar, M.; Anand, B.; Muthuvel, A.; Rajarajan, M.; Mohana, V.; Sundaramanickam, A. Enhanced Photocatalytic Dye Degradation and Antibacterial Activity of Biosynthesized ZnO-NPs Using Curry Leaves Extract with Coconut Water. *Nanotechnol. Environ. Eng.* **2020**, *5*, 29.
(40) Nafis, A.; Kasrati, A.; Azmani, A.; Ouhdouch, Y.; Hassani, L. Endophytic Actinobacteria of Medicinal Plant Aloe Vera: Isolation, Antimicrobial, Antioxidant, Cytotoxicity Assays and Taxonomic Study. *Asian Pac. J. Trop. Biomed.* **2018**, *8*, 513−518.
(41) Luthra, P. M.; Singh, R.; Chandra, R. Therapeutic Uses Of Curcuma Longa (Turmeric). *Indian J. Clin. Biochem.* **2001**, *16*, 153−160.
(42) Chatel, G. How Sonochemistry Contributes to Green Chemistry? *Ultrason. Sonochem.* **2018**, *40*, 117−122.
(43) Ocsoy, I.; Demirbas, A.; McLamore, E. S.; Altinsoy, B.; Ildiz, N.; Baldemir, A. Green Synthesis with Incorporated Hydrothermal Approaches for Silver Nanoparticles Formation and Enhanced Antimicrobial Activity against Bacterial and Fungal Pathogens. *J. Mol. Liq.* **2017**, *238*, 263−269.
(44) Senthilkumar, P.; Babu, S.; Jaishree, V.; Joshua Stephen, K.; Yaswant, G.; Ranjith Santhosh Kumar, D. S.; Nair, N. S. Solvothermal-Assisted Green Synthesis of Hybrid Chi-Fe_3O_4 Nanocomposites: A Potential Antibacterial and Antibiofilm Material. *IET Nanobiotechnol.* **2020**, *14*, 714−721.
(45) Patil, A. H.; Jadhav, S. A.; Gurav, K. D.; Waghmare, S. R.; Patil, G. D.; Jadhav, V. D.; Vhanbatte, S. H.; Kadole, P. V.; Sonawane, K. D.; Patil, P. S. Single Step Green Process for the Preparation of Antimicrobial Nanotextiles by Wet Chemical and Sonochemical Methods. *J. Text. Inst.* **2020**, *111*, 1380−1388.
(46) Nthunya, L. N.; Derese, S.; Gutierrez, L.; Verliefde, A. R.; Mamba, B. B.; Barnard, T. G.; Mhlanga, S. D. Green Synthesis of Silver Nanoparticles Using One-Pot and Microwave-Assisted Methods and Their Subsequent Embedment on PVDF Nanofibre Membranes for Growth Inhibition of Mesophilic and Thermophilic Bacteria. *New J. Chem.* **2019**, *43*, 4168−4180.
(47) Giri, R. K.; Chaki, S. H.; Khimani, A. J.; Patel, S. R.; Deshpande, M. P. Thermal Investigation of Nanospheres and Nanowhiskers of $CuInS_2$. *Eur. Phys. J. Plus* **2021**, *136*, 320.
(48) Helan, V.; Prince, J. J.; Al-Dhabi, N. A.; Arasu, M. V.; Ayeshamariam, A.; Madhumitha, G.; Roopan, S. M.; Jayachandran, M. Neem Leaves Mediated Preparation of NiO Nanoparticles and Its Magnetization, Coercivity and Antibacterial Analysis. *Results Phys.* **2016**, *6*, 712−718.

https://doi.org/10.1021/acsomega.1c03795
ACS Omega 2021, 6, 26533−26544

(49) Sharma, J. K.; Srivastava, P.; Ameen, S.; Akhtar, M. S.; Singh, G.; Yadava, S. Azadirachta Indica Plant-Assisted Green Synthesis of Mn_3O_4 Nanoparticles: Excellent Thermal Catalytic Performance and Chemical Sensing Behavior. *J. Colloid Interface Sci.* **2016**, *472*, 220−228.
(50) Avetisyan, A.; Markosian, A.; Petrosyan, M.; Sahakyan, N.; Babayan, A.; Aloyan, S.; Trchounian, A. Chemical Composition and Some Biological Activities of the Essential Oils from Basil Ocimum Different Cultivars. *BMC Complementary Altern. Med.* **2017**, *17*, 60.
(51) Ahmad, N.; Sharma, S.; Alam, M. K.; Singh, V. N.; Shamsi, S. F.; Mehta, B. R.; Fatma, A. Rapid Synthesis of Silver Nanoparticles Using Dried Medicinal Plant of Basil. *Colloids Surf., B* **2010**, *81*, 81−86.
(52) Surjushe, A.; Vasani, R.; Saple, D. Aloe Vera: A Short Review. *Indian J. Dermatol.* **2008**, *53*, 163−166.
(53) Ahmadi, O.; Jafarizadeh-Malmiri, H.; Jodeiri, N. Eco-Friendly Microwave-Enhanced Green Synthesis of Silver Nanoparticles Using Aloe Vera Leaf Extract and Their Physico-Chemical and Antibacterial Studies. *Green Process. Synth.* **2018**, *7*, 231−240.
(54) Logaranjan, K.; Raiza, A. J.; Gopinath, S. C. B.; Chen, Y.; Pandian, K. Shape- and Size-Controlled Synthesis of Silver Nanoparticles Using Aloe Vera Plant Extract and Their Antimicrobial Activity. *Nanoscale Res. Lett.* **2016**, *11*, 520.
(55) Yong, J. W.; Ge, L.; Ng, Y. F.; Tan, S. N. The Chemical Composition and Biological Properties of Coconut (Cocos Nucifera L.) Water. *Molecules* **2009**, *14*, 5144−5164.
(56) Elumalai, E.; Kayalvizhi, K.; Silvan, S. Coconut Water Assisted Green Synthesis of Silver Nanoparticles. *J. Pharm. BioAllied Sci.* **2014**, *6*, 241−245.
(57) Maghimaa, M.; Alharbi, S. A. Green Synthesis of Silver Nanoparticles from Curcuma Longa L. and Coating on the Cotton Fabrics for Antimicrobial Applications and Wound Healing Activity. *J. Photochem. Photobiol., B* **2020**, *204*, 111806.
(58) Li, M.; Zhao, R.; Su, Y.; Hu, J.; Yang, Z.; Zhang, Y. Hierarchically $CuInS_2$ Nanosheet-Constructed Nanowire Arrays for Photoelectrochemical Water Splitting. *Adv. Mater. Interfaces* **2016**, *3*, 1600494.
(59) Mousavi-Kamazani, M.; Salavati-Niasari, M.; Emadi, H. Synthesis and Characterization of $CuInS_2$ Nanostructure by Ultrasonic-Assisted Method and Different Precursors. *Mater. Res. Bull.* **2012**, *47*, 3983−3990.
(60) Patterson, A. L. The Scherrer Formula for X-Ray Particle Size Determination. *Phys. Rev.* **1939**, *56*, 978−982.
(61) Zhang, J.; Chen, J.; Li, Q. Microwave Heating Synthesis and Formation Mechanism of Chalcopyrite Structured $CuInS_2$ Nanorods in Deep Eutectic Solvent. *Mater. Res. Bull.* **2015**, *63*, 88−92.
(62) Xiao, J.; Xie, Y.; Tang, R.; Qian, Y. Synthesis and Characterization of Ternary $CuInS_2$ Nanorods via a Hydrothermal Route. *J. Solid State Chem.* **2001**, *161*, 179−183.
(63) Makuła, P.; Pacia, M.; Macyk, W. How To Correctly Determine the Band Gap Energy of Modified Semiconductor Photocatalysts Based on UV−Vis Spectra. *J. Phys. Chem. Lett.* **2018**, *9*, 6814−6817.
(64) Chaki, S. H.; Deshpande, M. P.; Tailor, J. P. Characterization of CuS Nanocrystalline Thin Films Synthesized by Chemical Bath Deposition and Dip Coating Techniques. *Thin Solid Films* **2014**, *550*, 291−297.
(65) Pamplin, B. R.; Kiyosawa, T.; Masumoto, K. Ternary Chalcopyrite Compounds. *Prog. Cryst. Growth Charact.* **1979**, *1*, 331−387.
(66) Angelov, M.; Goldhahn, R.; Gobsch, G.; Kanis, M.; Fiechter, S. Structural and Optical Properties of $CuInS_2$ Bulk Crystals. *J. Appl. Phys.* **1994**, *75*, 5361−5366.
(67) Das, D.; Nath, B. C.; Phukon, P.; Dolui, S. K. Synthesis and Evaluation of Antioxidant and Antibacterial Behavior of CuO Nanoparticles. *Colloids Surf., B* **2013**, *101*, 430−433.
(68) Thakor, P.; Subramanian, R. B.; Thakkar, S. S.; Ray, A.; Thakkar, V. R. Phytol Induces ROS Mediated Apoptosis by Induction of Caspase 9 and 3 through Activation of TRAIL, FAS and TNF Receptors and Inhibits Tumor Progression Factor Glucose 6 Phosphate Dehydrogenase in Lung Carcinoma Cell Line (A549). *Biomed. Pharmacother.* **2017**, *92*, 491−500.
(69) Gajera, S. B.; Mehta, J. V.; Thakor, P.; Thakkar, V. R.; Chudasama, P. C.; Patel, J. S.; Patel, M. N. Half-Sandwich Iridium (III) Complexes with Pyrazole-Substituted Heterocyclic Frameworks and Their Biological Applications. *New J. Chem.* **2016**, *40*, 9968−9980.
(70) Arunkumar, S.; Muthuselvam, M. Analysis of Phytochemical Constituents and Antimicrobial Activities of Aloe Vera L. against Clinical Pathogens. *World J. Agric. Sci.* **2009**, *5*, 572−576.
(71) Hu, Y.; Xu, J.; Hu, Q. Evaluation of Antioxidant Potential of Aloe Vera (Aloe Barbadensis Miller) Extracts. *J. Agric. Food Chem.* **2003**, *51*, 7788−7791.
(72) Saleh Al-Hashemi, Z. S.; Hossain, M. A. Biological Activities of Different Neem Leaf Crude Extracts Used Locally in Ayurvedic Medicine. *Pacific Sci. Rev. A: Nat. Sci. Eng.* **2016**, *18*, 128−131.
(73) Gülçin, İ.; Elmastaş, M.; Aboul-Enein, H. Y. Determination of Antioxidant and Radical Scavenging Activity of Basil (Ocimum Basilicum L. Family Lamiaceae) Assayed by Different Methodologies. *Phyther. Res.* **2007**, *21*, 354−361.
(74) Fonseca, A. M. d.; Bizerra, A. M. C.; Souza, J. S. N. d.; Monte, F. J. Q.; Oliveira, M. da C. F.; Mattos, M. C. d.; Cordell, G. A.; Braz-Filho, R.; Lemos, T. L. G. Constituents and Antioxidant Activity of Two Varieties of Coconut Water (Cocos Nucifera L.). *Rev. Bras. Farmacogn.* **2009**, *19*, 193−198.
(75) Meyer, B.; Ferrigni, N.; Putnam, J.; Jacobsen, L.; Nichols, D.; McLaughlin, J. Brine Shrimp: A Convenient General Bioassay for Active Plant Constituents. *Planta Med.* **1982**, *45*, 31−34.
(76) Simorangkir, M.; Nainggolan, B.; Juwitaningsih, T.; Silaban, S. The Toxicity of N-Hexane, Ethyl Acetate and Ethanol Extracts of SarangBanua (Clerodendrumfragrans Vent Willd) Leaves by Brine Shrimp Lethality Test (BSLT) Method. *J. Phys.: Conf. Ser.* **2021**, *1811*, 012053.
(77) Alsammarraie, F. K.; Wang, W.; Zhou, P.; Mustapha, A.; Lin, M. Green Synthesis of Silver Nanoparticles Using Turmeric Extracts and Investigation of Their Antibacterial Activities. *Colloids Surf., B* **2018**, *171*, 398−405.

https://doi.org/10.1021/acsomega.1c03795
ACS Omega 2021, 6, 26533−26544